Prabha Materials Science Letters
Vol. 4, No. 2, 179-196, 2025
https://doi.org/10.33889/PMSL.2025.4.2.017

Ram Arti Publishers

# SRIM/TRIM Analysis Reveals Depth-Dependent Damage Dynamics on Thin Tungsten Carbide by Employing low Energy and SHI

**Shivani Chaudhary**
Department of Physics,
Deen Dayal Upadhyaya Gorakhpur University, Gorakhpur, 273009, Uttar Pradesh, India.
E-mail: chaudharyshivi16jan@gmail.com

**Akanksha Gupta**
Department of Physics,
Deen Dayal Upadhyaya Gorakhpur University, Gorakhpur, 273009, Uttar Pradesh, India.
E-mail: guptaakanksha689@gmail.com

**Sakshi Singh**
Department of Physics,
Deen Dayal Upadhyaya Gorakhpur University, Gorakhpur, 273009, Uttar Pradesh, India.
E-mail: sakshi24janury@gmail.com

**Mukesh Kumar**
Department of Physics,
Deen Dayal Upadhyaya Gorakhpur University, Gorakhpur, 273009, Uttar Pradesh, India.
E-mail: mkjai426@gmail.com

**Vinay Kumar Srivastava**
Department of Physics,
Deen Dayal Upadhyaya Gorakhpur University, Gorakhpur, 273009, Uttar Pradesh, India.
E-mail: vinaypramod26@gmail.com

**Udai Bhan Singh**
Department of Physics,
Deen Dayal Upadhyaya Gorakhpur University, Gorakhpur, 273009, Uttar Pradesh, India.
*Corresponding author*: udaibhansingh123@gmail.com

(Received on January 19, 2025; Revised on March 7, 2025; Accepted on March 10, 2025)

**Abstract**
The Stopping Power Ranges of Ions in Matter (SRIM) and the Transport of Ions in Matter (TRIM) package are used to study ion irradiation and deceleration. The SRIM package provides insights into expected range and energy deposition through Monte Carlo simulations, while the TRIM package focuses on ion deceleration, sputtering events, atom recoils, and damage investigations. This manuscript investigates damages induced by a diverse range of ions, spanning from 10keV to 100 keV and 1MeV and 2 MeV Au ions on a 5nm thin layer of tungsten carbide using comprehensive TRIM computations with the Full Cascade Collisions. The research shows that nuclear stopping power is more prominent in deeper places, while electronic stopping is more prevalent near the surface. Low-energy ions lose a larger fraction of their energy to recoils than high-energy ions. The study also examines ion range features, damage profiles, flaws, and the damage range and production rate for various atomic species. The results greatly affect material engineering and ion beam applications.

**Keywords-** SRIM/TRIM, Low/high energy ion beam, Stopping power, Ion ranges, Damage energy.

## 1. Introduction

Within the domain of thin film engineering, the intricate relationship between surface modifications and the consequential displacement damage caused by low-energy ions represents a crucial boundary that demands careful consideration (Seitz, 1956). The present manuscript explores the intricate realm of theoretical exploration utilizing the Stopping Power Ranges of Ions in Matter (SRIM)/ Transport of Ions in Matter (TRIM) package (version 2008.04), with the objective of unraveling the intricate fabric of surface and displacement damage engineering (Ziegler and Biersack, 1985; Ziegler et al., 2010). During the process of traversing the intricate domains of sub-micron thin layers subjected to the impact of ions possessing low/high energy, our scientific endeavor uncovers the intricate interplays that dictate the material's reactions (Dhara, 2007; Eckstein, 2013). Our study begins with a look into the surface changes brought on by low/high-energy ions. We simulate the impacts of ion collision in great detail, shedding light on how the morphology, chemistry, and crystalline structure of the surface are altered (Eckstein, 2013). The information in this section is crucial for fine- thin layer surfaces for various uses. A considerable body of literature exists pertaining to the irradiation of nanostructures with high and low energy ions, with numerous publications documenting the resultant alterations in structure, composition, and electrophysical properties of the irradiated nanostructures (Ziegler et al., 2010). However, the process of irradiation can exert an influence not only on the alteration of properties, but also on the potential degradation of the structural integrity of nano-objects. The determination of localized regions within nanostructures, where the occurrence of maximum damage is anticipated, can be achieved through the utilization of computational models that simulate the intricate interplay between ions and the target material.

Tungsten carbide thin films find extensive application in protective coatings, microelectronics, and nuclear sectors, attributed to their remarkable hardness, higher melting point, and superior resistance to wear and corrosion (Zhu et al., 2018). Irradiation-induced modifications can significantly improve performance in extreme environments such as space applications, nuclear reactors, and cutting tools subjected to high irradiation fluxes (Racz et al., 2023). Modifications in structure can affect mechanical characteristics, phase stability, and conductivity, rendering them crucial for the advancement of material engineering (Bist et al., 2024). Numerous industrial uses, such as hobs, drills, cutting tools, armor-piercing rounds, and the aerospace and aeronautical sectors, also employ tungsten carbide thin films. Ion beam experiments can change the large-scale surface of tungsten and tungsten carbide, which improves their tribological properties, like how well they resist wear and friction (Aradi et al., 2018; Fogarassy et al., 2023). The process of ion beam mixing serves as a method for the fabrication of thin films and nanolayers, which are utilised in the development of protective coatings. The processes of ion implantation and ion beam mixing can modify the surfaces of tungsten carbide through the incorporation of metals, thereby altering its catalytic activity (Bist et al., 2024). Utilising combined electron-ion methodologies alongside pulsed electron beams presents a viable approach for modifying the surface characteristics of tungsten carbide pseudo-alloys (Zhu et al., 2018; Racz et al., 2023).

Energy deposition is the first step in the structural modification event, which causes atomic displacement in the lattice by impacting neighboring atoms and, ultimately, considerable stress in the lattice geometry (Mahne et al., 2022, 2023). In addition, vacancies and point defects are introduced into the lattice geometry as a consequence of atomic displacement (Mahne et al., 2022, 2023). Thus, the examination of collision events yields specific data on atomic displacement and vacancies. Furthermore, the displacement damage and displacement cross-section, both of which are relevant in the setting of low ion irradiation (Nordlund et al., 2018; Chen and Bernard, 2020), may be gleaned from collision event analysis. Again, atom recoil causes surface sputtering, which in turn causes surface alteration (Chen and Bernard, 2020; Mahne et al., 2022) Hence, for all these reasons, low energy ion irradiation may be employed as a technique to design the surface and displacement damage of the material. Tungsten carbides (WC) exhibit a diverse array of

both current and prospective applications within various industries (Seyyedhabashy et al., 2020). The tribological application of tungsten carbides as a wear and corrosion-resistant coating is attributed to its superior hardness, low friction coefficient, and thermal stability (Seyyedhabashy et al., 2020). Furthermore, it has found practical applications as a thin-film diffusion barrier and a Schottky contact in the field of high temperature electronics (Seyyedhabashy et al., 2020). In recent years, there has been a growing recognition of its significance as an electrocatalyst, thereby elevating its prominence (Shu et al., 2013).

The utilization of SRIM has been extensively employed by researchers to investigate various aspects such as depth profile, target damage, energy loss, and other phenomena resulting from ion irradiation (Ziegler et al., 2010; Eckstein, 2013). The Transport of Ions in Matter (TRIM) program focuses on the ion deceleration process. The TRIM software additionally offers data pertaining to atomic recoil, sputtering, and damage investigations (Ziegler et al., 2010; Eckstein, 2013). In this study, a comprehensive analysis of damage induced by full-cascade TRIM calculation has been conducted. TRIM (Chen and Bernard, 2020; Avanzi et al., 2022) is a highly popular simulation code within the ion beam community, primarily attributed to its user-friendly menu-driven software interface (Chen and Bernard, 2020; Avanzi et al., 2022). In this section, we will provide a concise overview of the TRIM code. The simulation accounts for the impact of ion irradiation on the target species by assuming a constant composition of the target layer throughout the simulation (Hofsäss et al., 2014; Nath and Das, 2021). The TRIM code exhibits the capability to simulate a wide range of effects resulting from ion irradiation, encompassing ion distribution, target damage, energy deposition caused by implanted ions, and more (Nath and Das, 2021). The simulation of ion-solid interaction is achieved through the utilization of the binary collision approximation (BCA) (Nath and Das, 2021).

This manuscript delves into the Stopping Power Ranges of Ions in Matter (SRIM) study, which investigates ion irradiation and energy deposition on tungsten carbide using Monte Carlo simulations. The TRIM package explores ion deceleration, sputtering events, and damage investigations. The study reveals a shift from electronic to nuclear stopping powers at different depths within the target, particularly at low ion energies. This manuscript provides a comprehensive understanding of the complex interplay between ion beams and Tungsten Carbide, spanning electronic and nuclear stopping powers, energy loss dynamics, ion range characteristics, and structural impacts. The findings have implications for material engineering and ion beam applications, offering a valuable resource for researchers in the field.

## 2. Materials and Simulation Methodology

SRIM/TRIM packages are useful instruments for interpreting the complex interaction between ions and a target material. Developed by Ziegler and released in 1985, this software pair explores the domain of ion-target interactions. The package Stopping Power Ranges of Ions in Matter (SRIM) focuses on important features of ion irradiation, such as expected range and energy deposition. It reveals the finer points of the physical processes involved via the use of a Monte Carlo simulation based on the binary collision approximation (BCA). Conversely, the TRIM package delves into the fascinating field of ion deceleration. Apart from its principal function of clarifying ion slowing down, TRIM offers vital insights into sputtering events, atom recoils, and the complexities of damage investigations. The present work investigates the damages caused by a variety of ions, namely 10keV to 2 MeV Au ions, on a 5nm thin layer of tungsten carbide (WC) using a Detailed calculation with Full damage Cascades TRIM computation. W and C were subjected to threshold displacement energies ($E_d$) of 25 eV and 20 eV, respectively.

## 3. Related Theories

The concept of "stopping power" in the context of ion beam irradiation on thin films pertains to the rate at which charged particles, such as ions, disperse energy while traversing a material. Additionally, it quantifies

the energy dissipation exhibited by the ions within the material relative to the length of their trajectory (Nastasi et al., 1996). The variables influencing the stopping power encompass the nature of the ions, their energy levels, and the inherent properties of the material composing the thin film. Accurate determinations of stopping power are of utmost significance in the realm of materials investigation, specifically within the domains of device fabrication and the alteration of material surfaces through ion beam manipulation. This is due to their integral role in augmenting our comprehensive understanding of the intricate interplay between ions and solids (Nastasi et al., 1996; Jain and Agarwal, 2011). Electronic and nuclear stopping are distinct constituents of the comprehensive stopping power experienced by ions as they traverse a substance. The phenomenon of energy dissipation exhibited by ions as a consequence of their interactions with electrons present in the target material is commonly denoted as electronic stopping. The phenomenon of energy dissipation exhibited by ions as a consequence of their interactions with the atomic nuclei of the target substance is commonly denoted as nuclear stopping. The total stopping is the sum of electronic stopping and nuclear stopping (Nastasi et al., 1996; Sigmund, 1981):

$$S = S_e + S_n \quad (1)$$

The comprehension of these constituents holds paramount importance in ion beam applications as it facilitates the anticipation of ion penetration depth within a material and provides profound understanding of the underlying physical phenomena, including but not limited to ion implantation, sputtering, and damage accumulation (Sigmund, 1981; Jain and Agarwal, 2011).

The amount of energy ΔE that an ion suffers a loss when travelling along a particular path x is a quantity with uncertainty, This means that different ions will lose varying amounts of energy (Bohr, 1913; Rautray et al., 2011).

The stopping power ($S$) is calculated using the average value of the energy loss i.e. $-\frac{\Delta E}{\Delta x}$. In the case of a significant number of ions. It is the total of the two energy losses and is provided by (Ramola et al., 2013):

$$S = \frac{-1}{\rho}\frac{dE}{dx} = S_e + S_n \quad (2)$$

Here, ($S_e$) and ($S_n$) denote the electronic and nuclear stopping powers, correspondingly, and ( $\rho$) represents the density of atom of the material.

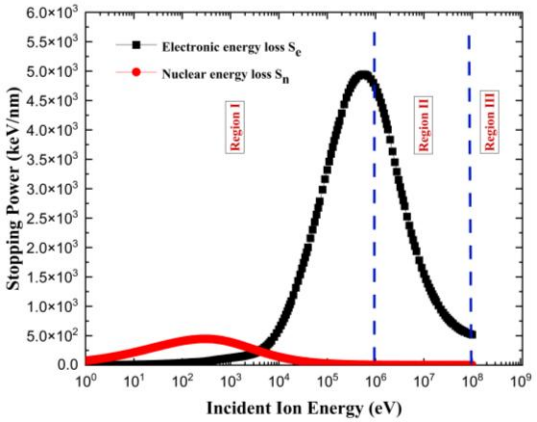


**Figure 1.** The energy loss variation of ions with the energy of the ion Ag in an Au target was calculated using SRIM-TRIM (Ziegler and Biersack, 2008, "SRIM-2008, stopping power and range of ions in matter").

### 3.1 Nuclear Energy Loss

Nuclear energy loss, denoted as "($S_n$", refers to the energy transferred when an ion collides elastically with lattice atoms in the target material, adhering to the principles of preserving momentum and energy. Because of their reduced frequency, these collisions are classified as binary collisions. At lower ion energies (0.1MeV/u), the nuclear energy loss mechanism is dominant.

There are two major assumptions that are taken into consideration in the calculation of nuclear energy loss:
i) An easy concealed Coulomb potential.
ii) Estimation of impulses.

The Coulomb potential of two atoms $Z_1$ and $Z_2$ may be expressed as $V = Z_1$ to screened Coulomb possible, when the impact parameter is significant, the nuclear charge is shielded by the electrons, leading to a modified scattering potential distinct from the unscreened Coulomb potential ($V = Z_1$) to the screened Coulomb potential ($V = Z_2$) (Bohr, 1913).

$$V(r) = \frac{Z_1 Z_2 e^2 \chi}{r}\left(\frac{r}{a}\right) \tag{3}$$

where, '$a$' is the collision's Thomas-Fermi screening radius.

$$a = \frac{0.885 a_0}{\left(Z_1^{\frac{1}{2}} + Z_2^{\frac{1}{2}}\right)^{\frac{2}{3}}} \tag{4}$$

For the majority of interactions, the values of '$a$' are between 0.1 Å and 0.2 Å. The screening function in Moliere approximation can be defined as:

$$\chi\left(\frac{r}{a}\right) = \frac{a}{2r} \tag{5}$$

The impulse approximation is well-suited for collisions characterized by small angles and large impact parameters, which predominantly govern the scattering process that determines the trajectory of charged particles. The cross section ($d\sigma$) for energy transfer between $T$ and $T + dT$ is given by using the impulse approximation and screened Coulomb potential.

$$d\sigma = \pi \frac{Z_1 Z_2 e^2 a}{8\sqrt{\left(\frac{M_2}{M_1}\right)E}} T^{\frac{3}{2}}\, dT \tag{6}$$

If projectile ions, which usually have energies of several keV per nucleon, contact with screened or unscreened target atom nuclei, the likelihood ($P(E)$) that an energetic particle (E) will transmit some energy to the target atom (in range of $T$ and $T + dT$) is given by:

$$\frac{dP(E)}{dT} dT = N dx \frac{d\sigma(E)}{dT} dT \tag{7}$$

The mean energy loss throughout a distance ($dx$) of a moving particle is calculated:

$$\langle dE \rangle = \int T \frac{dP(E)}{dT} dT = N \int T \frac{d\sigma(E)}{dT} dT \tag{8}$$

The nuclear energy loss for tiny *dx* is:

$$\left[\frac{dE}{dx}\right]_n = N \int_{T_{min}}^{T_{max}} T \frac{d\sigma(E)}{dT} dT \tag{9}$$

The integration's power limit $T_{min}$ is the minimal amount of energy transmitted, and it must be zero. $T_{max}$ is defined as the highest amount of energy that may be transferred and demonstrated by:

$$T_{max} = 4\ \frac{M_1 M_2}{(M_1+M_2)^2}\ E \tag{10}$$

Here, $M_1$ and $M_2$ are the masses of the target atom and the projectile ion, correspondingly. Equation (9) is used to get the formula for nuclear energy loss, the values of $(d\sigma)$ and $(T_{max})$ are taken from Equations (6) and (10), correspondingly:

$$\left[\frac{dE}{dx}\right]_n = N\frac{\pi^2 Z_1 Z_2 e^2 a}{2}\frac{M_1}{(M_1+M_2)} \tag{11}$$

The endowment of nuclear energy dropping in the higher energy domain is negligible.

### 3.2 Electronic Energy Loss

Electronic energy loss, denoted as $(S_e)$, occurs due to energy transfer from electronic collisions when an ion interacts interacting with electrons inside atomic lattices, resulting in ionization and excitation. This kind of collision happens often and is usually inelastic.

According to Bohr and others, a straightforward criterion assumes that ions lose electrons only from orbits where the orbital velocity $(V_o)$ is less than the velocity of the projectile ion $(V_I)$. This results in an effective charge (Frost et al., 2000) on the projectile, which can be calculated as follows:

$$\frac{Z^*}{Z_I} = \frac{V_I}{V_o Z_I^{\frac{2}{3}}} \tag{12}$$

where, $Z^*$ represents the ion's effective charge and $Z_I$ represents the total number of electrons associated with the ion in its ground state. Additionally, experimental evidence has shown the ion charge fraction for a heavy ion to be:

$$\frac{Z^*}{Z_I} = 1 - exp\left(\frac{0.92 V_I}{Z^{\frac{2}{3}} V_o}\right) \tag{13}$$

According to equation (13), there are two limiting situations depending on the velocity of the ion:

**CASE- I**

When the ion's velocity is smaller than the orbital velocity of electrons $(V_I < V_0)$ and $\frac{Z^*}{Z_I} < 1$, as seen in area that the projectile (ion) encounters electron clouds around each target atom on its journey.

The Lindhard-Scharff electronic stopping cross-section is given by:

$$S_{LS}(E) = \xi_L 8\pi e^2 a_0 N.\frac{Z_I Z_T}{\left(Z_I^{\frac{2}{3}}+Z_T^{\frac{2}{3}}\right)^{\frac{2}{3}}}\left(\frac{V}{V_o}\right) = K_L E^{\frac{1}{2}} \tag{14}$$

The correction factor is, where $Z_I$ and $Z_T$ are the charges corresponding to the projectile ion and target atom, respectively. The elementary charge is $E$, and the typical Bohr radius is $a_0$.

$$\left[a_o = \frac{\hbar^2}{(m_e e^2)}\right] \tag{15}$$

The velocity seems to be proportionate to the electronic stopping cross-section or $E^{\frac{1}{2}}$ of the projectile ion, as shown by Equation (14).

**CASE- II**

When the ion's velocity is equal to or greater than the orbital velocity of electrons ($V_I > V_0$) As mentioned in **Figure 1** (Region III) [Completely stripped case $\frac{Z^*}{Z_I} > 1$].

As the velocity of the projectile/ion increases, the amount of time it spends close to an atom decrease, resulting in a decrease in the stopping cross-section. The Bethe-Bloch formula may be used to characterize the dependency of electronic energy loss on non-relativistic ions.

$$S_{BB}(E) = \frac{8\pi Z_I^2 e^4}{I_o \in B_2} ln \in_B \quad (16)$$

where, $\in_B = \frac{2m_e V_I}{Z_T I_o}$ and $I_o$ is the target's mean excitation energy as provided by:

$I_o = 12 + 7\ Z_T^{-1}(eV)$ For ZT < 13

$I_o = 9.76 + 58.5 Z_T^{-1.19}(eV)$ For ZT >13

Equation (16) may be written as a first approximation as:

$$S_{BB}(E) \propto \frac{1}{E} \propto \frac{1}{V_1^2} \quad (17)$$

As an initial approximation of the Bethe-Bloch formulation described by Equation (17), As the velocity of the projectile ions increases, the electronic stopping cross-section reduces.

Low and high electronic stopping power regimes are distinguishable from one another. The stopping power is directly proportional to $V_I$ in the low domain, when the projectile ion is just partly ionized. High is where it is completely stripped, resulting in an inverse square relation of stopping power with velocity. In general, electronic stopping power has a higher stopping power than mechanical stopping power.

### 3.3 Projected Range and Range Distribution

The projected range can be defined as the mean displacement covered by an ion within a material prior to reaching a state of rest. This particular statistical measure serves as a means to estimate the depth of ion penetration. In the realm of SRIM/TRIM simulations, the determination of the projected range frequently entails the utilization of the stopping power in conjunction with the material's density (Singh and Rout, 2021). The projected range $R_p$ is given by the formula (Jain and Agarwal, 2011):

$$R_p = \int_0^{E_0} \frac{1}{S(E)} dE \quad (18)$$

Here, $E_0$ is the initial energy of of the ion, $S(E)$ is the stopping power as a function of ion energy.

The range distribution is a statistical representation of the distribution of ion ranges within a given material. It offers insights into the distribution of ion penetration depths. The range distribution is typically acquired by means of Monte Carlo simulations within the SRIM/TRIM framework (Ziegler et al., 2010; Singh and Rout, 2021). By aggregating data obtained from numerous simulated ion trajectories, a distribution of ranges is generated. A distribution of stopping points, also known as a range distribution, should exist. These distributions are defined by the mean ion range of the distribution function, which includes measures

such as skewness and kurtosis (Sigmund, 1981; Lawrence and Justin, 2011; Sigmund, 2014). Detailed calculation with Full damage Cascades TRIM is occasionally utilized to perform intricate calculations regarding the damage caused by ion bombardment. The formation and accumulation of point defects in the material are accounted for in this model (Chee et al., 2011).

### 3.4 Damage Energy and Displacement (dpa)

Within the domain of SRIM/TRIM simulations, the theory of displacements provides valuable insights into the structural modifications caused by ion beam irradiation by encapsulating the dynamic interplay between vacancies and replacement collisions (Chen and Bernard, 2020). Fundamentally, the equation Displacements = Vacancies + Replacement Collisions, elucidates the intricacies of interactions between ions and solids (Weber and Zhang, 2019; Chen and Bernard, 2020).

The concept of "displacements" pertains to the overall count of atoms that are energetically dislodged from their lattice positions within the target material as a result of ion beam irradiation (Nordlund et al., 2015). Conversely, vacancies manifest in the crystal structure when a recoiling atom, which has been ignited by collision events, abandons its initial lattice position, thereby creating a vacant or void. In addition, Specific conditions give rise to replacement collisions (Agarwal et al., 2021):

i) An atom in motion strikes a stationary target atom.
ii) More energy is transferred by the moving atom than is necessary to displace the target atom.
iii) The energy of the initial atom is inadequate to sustain its trajectory.
iv) The target and initial atoms belong to the identical elemental species.
v) Replacement collisions occur when a stationary target atom is seamlessly replaced by a moving atom in the lattice; this causes a structural transition that does not involve the formation of a vacancy.

Atomic collisions cause the incident ion to transmit kinetic energy to the target atoms, which are immobile, during irradiation. This causes the target atom to rebound; it is called a primary knock-on atom ($PKA$) and it has an initial kinetic energy ($E_{PKA}$) (Agarwal et al., 2021). Electronic excitation processes dissipate some of the $E_{PKA}$ by reducing the kinetic energy accessible to atomic displacements caused by collisions with other atoms in the target, as a result of interactions with the target's electrons (Agarwal et al., 2021). The damage energy ($T_{dam}$) is the amount of energy that remains after the photon displaced the atom and is transmitted to other atoms in the target by means of elastic collisions (Agarwal et al., 2021). French, Nelson, and half-Nelson models, as well as their British and American counterparts, were among the several Kinchin and Pease variants that circulated in the early 1970s. With a variance of around 30% among them, these models predicted half as many displacements as the original Kinchin-Pease model (Etherington et al., 1975; Dupouy, 1977; Stoller et al., 2013). To enable precise computer modeling of high-energy displacement cascades, Robinson and Torrens unveiled the MARLOWE binary collision code in 1974 (Stoller, 2012; Stoller et al., 2013). For a Primary Knock-On Atom ($PKA$) with a given energy, Norgett, Robinson, and Torrens ($NRT$) later created a secondary displacement model within the MARLOWE framework to determine the dpa (Stoller et al., 2013; Nordlund et al., 2015). As a result of its widespread acceptance within the field of radiation impacts, the $NRT$ model is now considered to be the preferred method for calculating atomic displacement rates (Robinson, 1994; Stoller et al., 2013).

A Primary Knock-On Atom ($PKA$) with kinetic energy $E_{PKA}$ generates a total of stable Frenkel pairs, which may be described as: according to the $NRT$ displacement model (Etherington et al., 1975; Stoller et al., 2013).

The following equation is a good approximation for Displacement (dpa) (Bratchenko et al., 2013; Stoller et al., 2013):

$$\vartheta_{NRT} = 0.8 \times \frac{T_{dam}}{2E_d} \quad (19)$$

$T_{dam}$ is the damage energy, denoted as $T_{dam}$, is the part of the $PKA$ energy ($E_{PKA}$) that is lost in elastic collisions with atoms in the lattice (Robinson, 1994). The full cascade TRIM option utilizes SRIM-predicted electronic stopping powers, ZBL scattering cross-sections, and employs a Monte Carlo method to track each primary knock-on atom ($PKA$) generated by an incident ion, as well as all secondary recoiling atoms, until their energy diminishes to a level insufficient to initiate further displacement events (i.e., when the recoiling energy, $E_{recoil}$, falls below the threshold displacement energy, $E_d$, for all target elements) (Robinson, 1994). The damage energy profiles were determined by analyzing the PHONON.TXT files for both full-cascade and quick TRIM simulations (Weber and Zhang, 2019). These files provide information about the total energy lost to phonons by the incident ion and the target recoils at different depths (Weber and Zhang, 2019). When it comes to quick TRIM, one can calculate the damage energy profile by analyzing the E2RECOIL.TXT and IONIZ.TXT files ( Weber and Zhang, 2019). This involves comparing the energy transferred to recoils with the energy lost by recoils to ionization at different depths. When considering full-cascade TRIM, it is possible to estimate the damage energy profile by using the displacement profile (Weber and Zhang, 2019). This profile is usually obtained by combining the information from the VACANCY.TXT and NOVAC.TXT files ( Weber and Zhang, 2019). The value of $T_{dam}$ can be also calculated by subtracting the energy lost to ionization by the incident ion and the recoils from the incident ion's energy. All these methodologies produce profiles that are statistically similar, with any differences being attributed to the energy binning process ( Weber and Zhang, 2019).

## 4. Results Discussion

### 4.1 Calculation using SRIM

Implementing Stopping Range, The SRIM calculation table for stopping powers versus energy and stopping powers versus depth of ions is provided below.

**Ion details-** Ion – Gold (Au), Atomic Number- 79, Atomic Mass- 196.67 amu.
**Target Composition-** Target- 5nm Tungsten Carbide (WC), Density- 15.63gm/cm.

In **Figure 2**, it is evident that the phenomenon of electronic stopping dominates over the nuclear stopping power as one progress deeper into the target from its surface. However, it is worth noting that as we transition from the surface to the deeper regions of the target, the dominance of nuclear stopping power over electronic stopping power becomes apparent. Moreover, it can be observed from **Figure 3** that the nuclear stopping power dominates over the electronic stopping power when considering ion beams with extremely low energy levels (specifically, in the range of a few kiloelectron volts, approximately >10 keV). However, in the realm of high energy (specifically, greater than 1 MeV), it is the electronic stopping power that takes precedence over the nuclear stopping power.

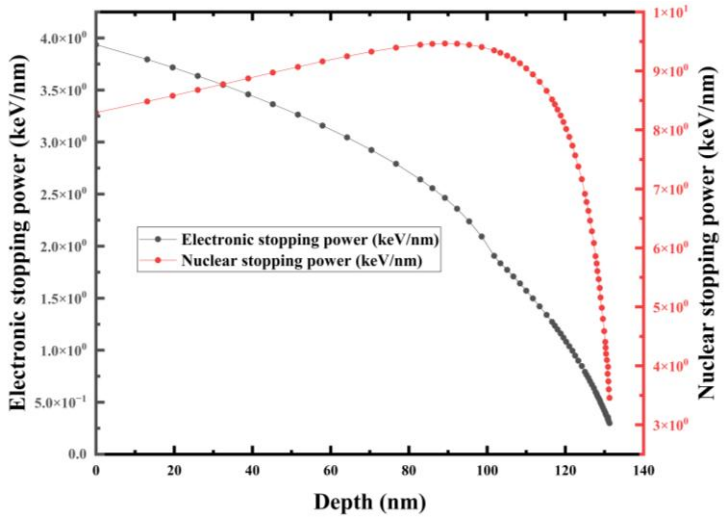


**Figure 2.** Demonstration of electronic and nuclear stopping power versus depth for 10keV to 2MeV Au ions on 5nm tungsten carbide (WC).

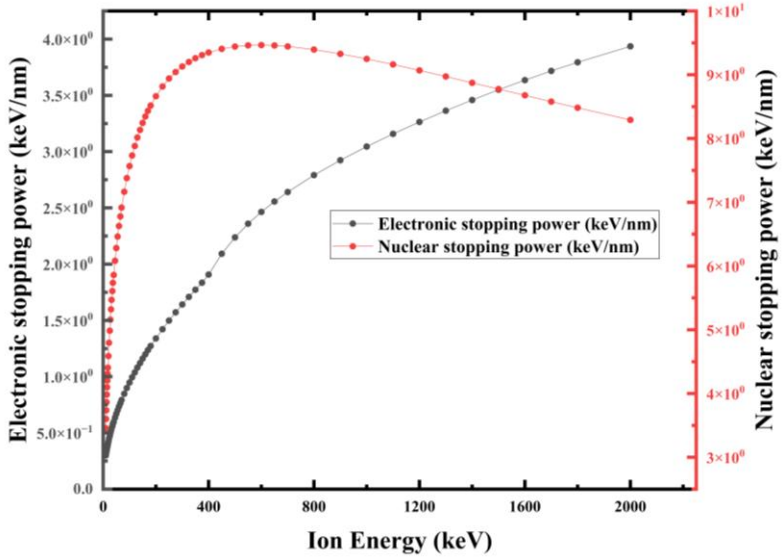


**Figure 3.** Demonstration of electronic and nuclear stopping power versus ion energy for 10keV to 2MeV Au ions on 5nm tungsten carbide (WC).

## 4.2 Calculation using TRIM

Results obtained from TRIM for 10keV, 100 keV, 1MeV and 2MeV Au ions on Tungsten Carbide (WC) are discussed in depth in this section. Here the graphical findings are explained using a variety of distribution curves, including range, concentration against depth, and energy loss per ion versus depth.

Important results include phonon and vacancy creation, as well as the amount of energy lost to ionization.

### 4.2.1 Energy Loss during Ionization

Energy loss-target depth curves derived from the comprehensive computation of full cascade collisions for the WC atoms' ionization by the incident Au ions with energies of 10 keV, 100 keV, 1 MeV, and 2 MeV are shown in **Figures 4 (a), (b), (c),** and **(d).** Loss of energy to the electrons that is relevant is called ionization. "Ions" data represents the energy transmitted directly from the Au-ion to the Tungsten Carbide, while "Recoils" data represents the energy transferred to the electrons of recoiling WC atoms. The energy loss to WC target phonons may be broken down into two parts: the first part is the %energy lost when the Au-ion creates phonons, and the second part is the %energy lost when WC recoiling atoms become phonons. Thus, phonons might originate from a variety of places. The product of the total ion energy and the total percentage of phonons yields the keV energy of phonons for each incident ion. The target may get very hot if phonons are assumed to directly contribute to the target temperature. For 10 keV Au ions, the TRIM calculation shows an energy loss of 15.06% during ionization and 51.23% during recoil while the energy of phonons per incident ion is 300 keV; for 100 keV Au ions, the energy loss is 29.34% during ionization and 48.10% during recoil while the energy of phonons per incident ion is 2.024 MeV. The energy loss due to ions is 66.41%, and the recoil energy loss is 24.55% for high-energy 1 MeV Au ions and 76.04% and 17.82%, respectively, for 2 MeV Au ions. The energy of phonons per incident ion is 7.9 MeV for 1 MeV Au ions and 10.88 MeV for 2 MeV Au ions. This suggests that, in comparison to high-energy ions, low-energy ions result in a smaller percentage of ion energy loss and a larger percentage of recoils.

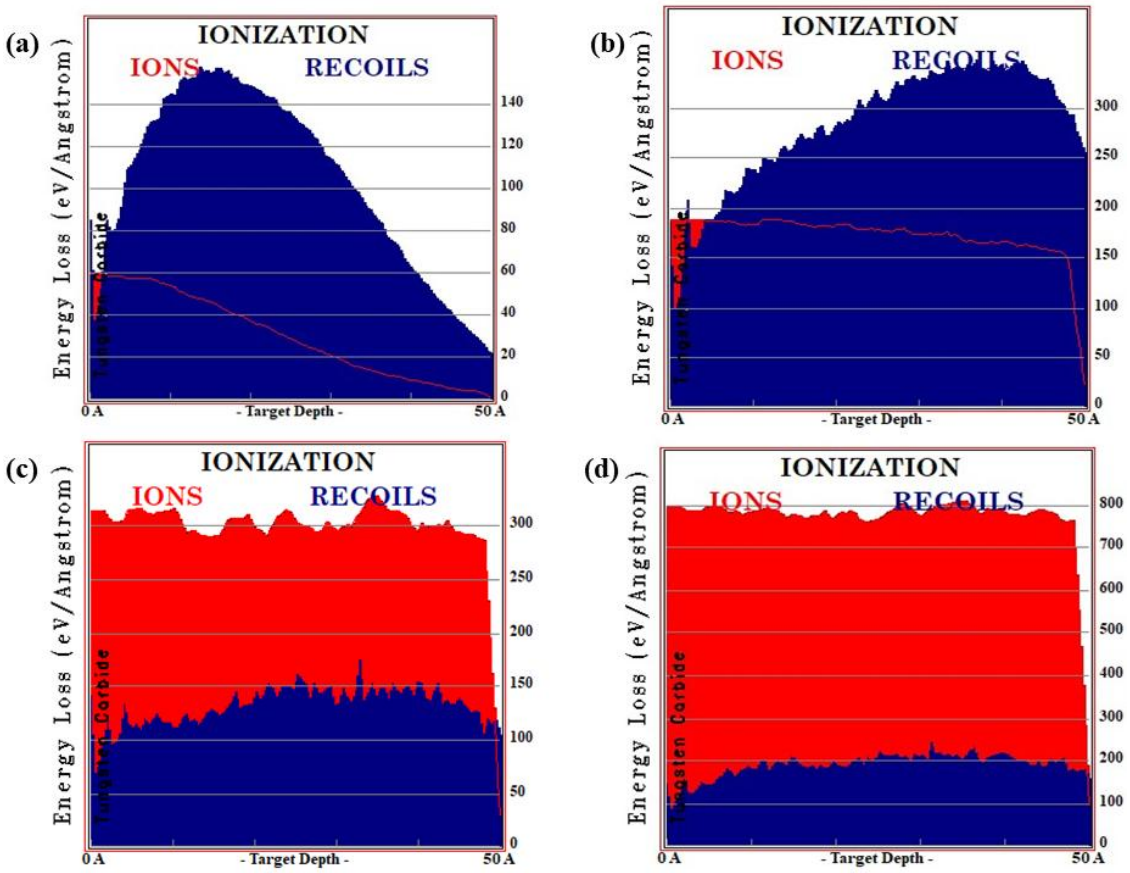


**Figure 4.** Ions and recoils ionization curves for (a) 10 keV, (b) 100 keV, (c) 1 MeV, and (d) 2MeV Au ions on tungsten carbide.

### 4.2.2 Ion Ranges

**Figures 5 (a), (b), (c),** and **(d)** below, depict the ion range characteristics observed when low and high energy Au ions are irradiated onto a Tungsten Carbide target. The ions possess energies of 10 keV, 100 keV, 1 MeV, and 2 MeV, respectively. The investigation focuses on the target depth of 50 Å. In this particular simulation procedure, we have simulated low-energy Au ions with kinetic energies of 10keV and 100keV within the ion range of the WC target, specifically spanning 28 Å and 29 Å. The corresponding straggles for these ions are measured to be 12 Å and 12 Å, respectively. On the other hand, we have for high-energy Au ions with kinetic energies of 1 MeV and 2 MeV within the same WC target ion range, which spans 23 Å and 21 Å. The straggles observed for these high-energy ions are measured to be 12 Å and 13 Å, respectively. Skewness quantifies the degree of symmetry exhibited by a peak. The value is null for systems exhibiting symmetry. The observed skewness values for Au ions with energies of 10 keV and 100 keV are -0.1750 and -0.3066, respectively. These coefficients exhibit a negative polarity. This implies that the negative tail of the distribution exhibits greater length compared to the positive tail, thereby resulting in a leftward skew of the graph. Kurtosis quantifies the degree to which the distribution of data deviates from a standard normal distribution, indicating whether it exhibits a more pronounced peak or a flatter shape. A numerical range spanning from 0 to 3 corresponds to a distribution exhibiting a lower degree of variation, while a value surpassing 3 signifies a distribution that is more concentrated around a central point. In our simulations, we have computed the kurtosis values for the curves corresponding to low energies (10 keV and 100 keV Au ions) and high energies (1 MeV and 2 MeV Au ions) interacting with WC. The kurtosis values obtained are 2.8729 and 2.0351 for low energies, and 2.0340 and 1.3281 for high energies, respectively. This positive kurtosis implies that the distribution exhibits tails that are more pronounced or heavier compared to the standard normal distribution. The kurtosis values lie within the range of 0 to 3, indicating the presence of distributions with decreased peakedness (that means flatter). Meanwhile, the skewness coefficients for the curve, specifically for 1 MeV and 2 MeV Au ions, are determined to be 0.5285 and 0.2503 respectively, both of which possess positive values. This positive skewness implies that the distribution's right tail extends further than its left, thereby indicating a rightward skew in the graph.

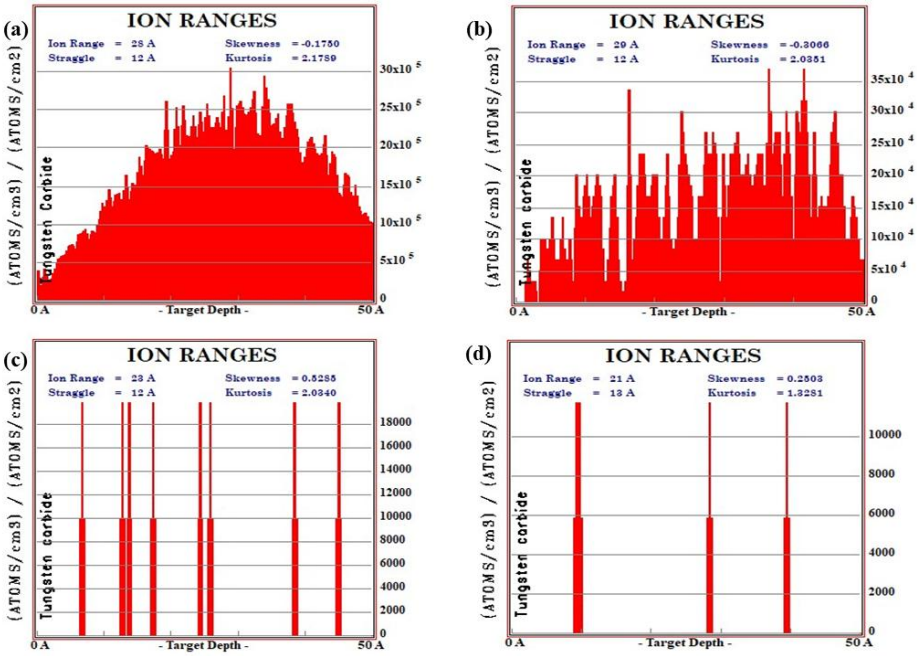


**Figure 5.** Ion range distribution for (a)10 keV, (b) 100 keV, (c) 1 MeV and (d) 2MeV Au ion in tungsten carbide.

### 4.2.3 Damage Energy and Displacement (dpa)

In particular, the displacement per atom (dpa) is one of the material's structural characteristics that could be affected by ion beam irradiation. In the "Detailed calculation with Full damage cascade" option of the SRIM-2008 program, we used the Detailed calculation with Full damage Cascades TRIM computation and a displacement threshold energy ($E_d$) of 25 eV to model the displacement damage profile. W and C were subjected to threshold displacement energies of 25 eV and 20 eV, respectively. As with other light element targets like Be, C, Si, and GaN, Carbide will not be involved in displacement and damage profiles due to its low atomic number (Chang et al., 2014; Fogarassy et al., 2023).

By using the Collision events, which cause atoms to move from their lattice locations, help understand the interaction between ions and a target sample. This research is crucial as the ion interacts with the atomic configuration, changing its path through electronic and nuclear scattering. The electrical and nuclear stopping power of the ion and the density of the target atom influence collision dynamics. Collision defects, such as vacancies and point defects, are created when atoms in the lattice undergo displacement. Investigating collision events helps understand ion propagation within a material. The displacement or knocking on of a target atom causes a cascade collision, resulting in high-energy particles and surface sputtering. Recoiling atoms also contribute to this cascade. Thus, target displacement, vacancies, and replacement collisions make up the overall collision event as a function of sample depth. We used the sum of incident ion's and the target's recoils' energy lost to phonons at each incremental depth, the damage energy profiles were achieved from the PHONON.TXT data used in full-cascade TRIM simulations.

In order to compare corresponding displacement profiles (dpa), the NRT model $\vartheta_{NRT} = 0.8 \times T_{dam}/2E_d$ was used to full-cascade damage energy profiles. **Figure 6** and **7** shows the damage profile vs depth, whereas **Figure 8** and **9** shows the peak displacement (dpa) damage at 2.05, 2.2 nm and 2.7, 2.4 nm for 5 nm WC exposed to low-energy Au ions (10 keV, 100 keV) and high-energy Au ions (1 MeV, 2 MeV), respectively. Defects such grain boundaries and dislocation clusters have formed in the sample, as seen by this ion beam-induced damage profile. The total number of target displacements $\vartheta_{fc}$ are 133/ion, 255/ion, 140/ion and 126/ion for low energies (10 keV, 100 keV) and high energies (1 MeV, 2 MeV) Au ions on 5 nm WC, respectively.

Most importantly, the damage range reveals information on how far into the sample defects originate. Damage profiles in **Figures 6 and 7** are also asymmetrical; for low energies (10 keV, 100 keV) and high energies (1 MeV, 2 MeV) Au ions on 5 nm WC, respectively, the damage constantly declines following the peak at 3.2 nm, 2.1 nm, 3.4 nm, and 2.7 nm.

The depth and form of the damage profiles are affected by forward scattering, which is appropriately compensated in the full-cascade models. They also offer the damage production rate for various atomic species in multi-elemental targets. Ion beam irradiation changes lattice spacing and tension, which leads to an asymmetrical damage profile. We clearly observed from the **Figures 6** and **7** that, in the case of high energies, the damage energy profiles are shifted to greater depths; however, there is not much shift in the depth for the low energies. The damage percentage by calculating average of percent integral area under the curve in damage profiles are 16.57%, 14.28%, 9.09% and 10.10% for low energies (10 keV, 100 keV) and high energies (1 MeV, 2 MeV) Au ions on 5 nm WC, respectively. This is strongly related to the energy deposition that causes displacement damage and also due to dominance of nuclear or electronic stopping. **Figure 10** and **11** shows the linear increment graph of Displacement (dpa) versus Damage energy(keV/nm).

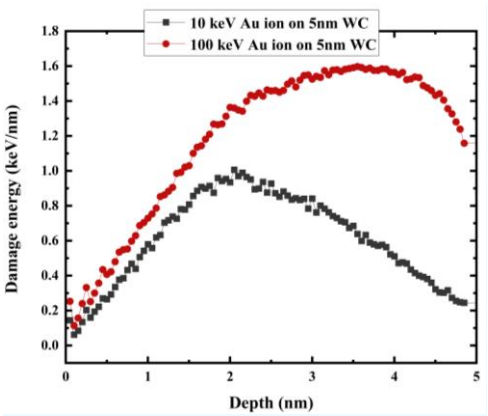


**Figure 6.** Damage energy profiles derived from the full cascade TRIM simulations, as a function of depth for 10 keV and 100 keV, Au ion on tungsten carbide.

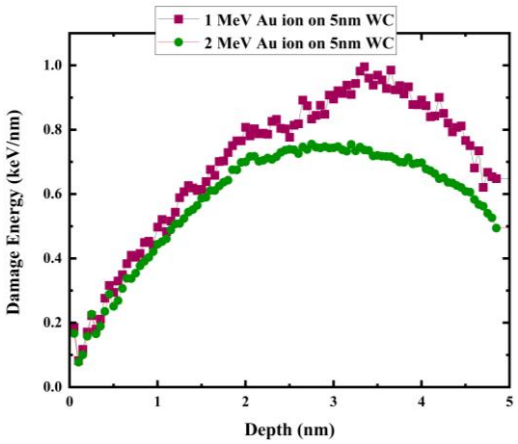


**Figure 7.** Damage energy profiles derived from the full cascade TRIM simulations, as a function of depth for 1 MeV and 2 MeV, Au ion on tungsten carbide.

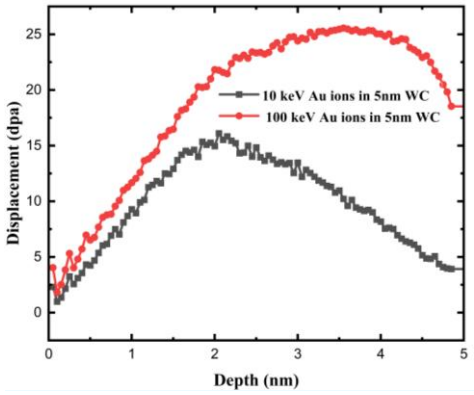


**Figure 8.** Displacement profiles (dpa) from the full cascade TRIM simulations, predicted using the NRT model, as a function of depth, for 10 keV and 100 keV, Au ion on tungsten carbide.

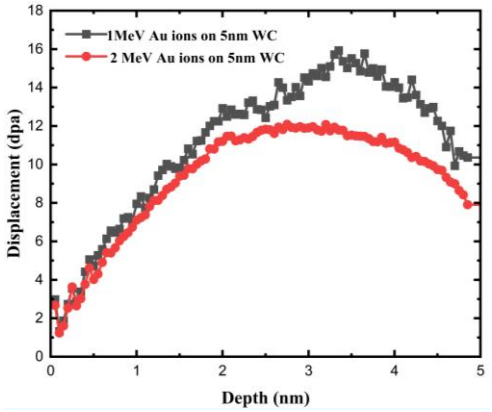


**Figure 9.** Displacement profiles (dpa) from the full cascade TRIM simulations, predicted using the NRT model, as a function of depth, for 1 MeV and 2 MeV, Au ion on tungsten carbide.

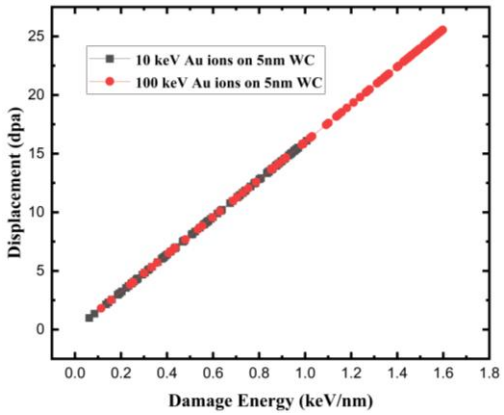


**Figure 10.** The relationship between damage energy and the number of atoms displaced in full cascade TRIM and NRT models 10 keV and 100 keV, Au ion on tungsten carbide.

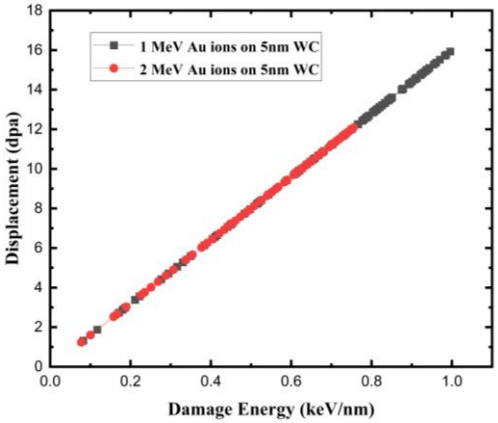


**Figure 11.** The relationship between damage energy and the number of atoms displaced in full cascade TRIM and NRT models 1 MeV and 2 MeV, Au ion on tungsten carbide.

## 5. Conclusion

The study investigates ion beam irradiation on Tungsten Carbide, revealing the interplay between electronic and nuclear stopping powers at varying depths within the target. The dominance shifts from electronic to nuclear stopping power is observed as we transition from the surface to deeper regions, with a notable reversal at extremely low ion energies. The distribution of energy loss to electrons during ionization and recoils in Tungsten Carbide is highlighted, with low-energy ions exhibiting a smaller percentage of energy loss to ions and a larger percentage to recoils. Ion range characteristics are also examined, with skewness and kurtosis analyses providing a comprehensive understanding of the ion range dynamics. The study also explores the structural effects of ion beam irradiation, with displacement damage profiles showcasing the formation of defects such as grain boundaries and dislocation clusters. The analysis of damage range and percentage further elucidates the depth and extent of defect formation within the sample. The study contributes to the understanding of ion-target interactions and offers practical insights for material engineering and ion beam applications.

### Conflict of Interest

The authors confirm that there is no conflict of interest to declare for this publication.

### AI Disclosure

The author(s) declare that no assistance is taken from generative AI to write this article.

### Acknowledgments

One of the authors (Shivani Chaudhary) is thankful to the IUAC (through project fellow UFR-67318) & and UBS also grateful to SERB-SURE project [project no. SUR/2022/004428].

## References

Agarwal, S., Lin, Y., Li, C., Stoller, R.E., & Zinkle, S.J. (2021). On the use of SRIM for calculating vacancy production: quick calculation and full-cascade options. *Nuclear Instruments and Methods in Physics Research Section B: Beam Interactions with Materials and Atoms*, *503*, 11-29.

Aradi, E., Lewis-Fell, J., Harrison, R.W., Greaves, G., Mir, A.H., Donnelly, S.E., & Hinks, J.A. (2018). Enhanced radiation tolerance of tungsten nanoparticles to He ion irradiation. *Nanomaterials*, *8*(12), 1052.

Avanzi, L.H., Aguiar, V.A.P., Costa, K.M., Santarelli, T.O., Medina, N.H., Oliveira, J.R.B., Cappuzzello, F., Iazzi, F., Capirossi, V., Pinna, F., Cavallaro, M., Guazzelli, M.A. (2022). Using TRIM-SRIM code simulations to determine defect density produced in HOPG irradiated with high energy heavy ions. In *Journal of Physics: Conference Series* (Vol. 2340, No. 1, p. 012002). IOP Publishing, Brazil.

Bist, S., Kalita, P., Shah, S., Singh, N., Gupta, R., Sulania, I., & Avasthi, D.K. (2024). Swift heavy ion irradiation effects on tungsten carbide films. *Journal of Alloys and Compounds*, *976*, 173201. https://doi.org/10.1016/j.jallcom.2023.173201.

Bohr, N. (1913). I. On the constitution of atoms and molecules. *The London, Edinburgh, and Dublin Philosophical Magazine and Journal of Science*, *26*(151), 1-25.

Bratchenko, M.I., Bryk, V.V., Dyuldya, S.V., Kalchenko, A.S., Lazarev, N.P., & Voyevodin, V.N. (2013). Comments on DPA calculation methods for ion beam driven simulation irradiations. *Ukrain*, *2*(10), 11-16.

Chang, J., Cho, J.Y., Gil, C.S., & Lee, W.J. (2014). A simple method to calculate the displacement damage cross section of silicon carbide. *Nuclear Engineering and Technology*, *46*(4), 475-480.

Chee, F.P., Amir, H.F.A., & Salleh, S. (2011). Simulation of ionizing radiation induced effects in nanoscale semiconductor material. In *2011 IEEE Regional Symposium on Micro and Nano Electronics* (pp. 245-249). IEEE. Kota Kinabalu, Malaysia.

Chen, S., & Bernard, D. (2020). On the calculation of atomic displacements using damage energy. *Results in Physics*, *16*, 102835.

Dhara, S. (2007). Formation, dynamics, and characterization of nanostructures by ion beam irradiation. *Critical Reviews in Solid State and Materials Sciences*, *32*(1-2), 1-50.

Dupouy, J.M. (1977). *French program on LMFBR cladding materials development*. American Institute of Mining, Metallurgical, and Petroleum Engineers, Inc., New York.

Eckstein, W. (2013). *Computer simulation of ion-solid interactions* (Vol. 10). Springer Science & Business Media, New York.

Etherington, E.W., Bramman, J.I., Nelson, R.S., & Norgett, M.J. (1975). A ukaea evaluation of displacement damage models for iron. *Nuclear Engineering and Design*, *33*(1), 82-90.

Fogarassy, Z., Kentsch, U., Panjan, P., & Racz, A.S. (2023). Experimental and theoretical study on the production of carbide-rich composite nano-coatings. *Surfaces and Interfaces*, *38*, 102773. https://doi.org/10.1016/j.surfin.2023.102773.

Frost, F., Schindler, A., & Bigl, F. (2000). Roughness evolution of ion sputtered rotating InP surfaces: pattern formation and scaling laws. *Physical Review Letters*, *85*(19), 4116.

Hofsäss, H., Zhang, K., & Mutzke, A. (2014). Simulation of ion beam sputtering with SDTrimSP, TRIDYN and SRIM. *Applied Surface Science*, *310*, 134-141.

Jain, I.P., & Agarwal, G. (2011). Ion beam induced surface and interface engineering. *Surface Science Reports*, *66*(3-4), 77-172.

Lawrence, A.L., & Justin, M.W. (2011). Ion implantation of semiconductor doping and material modification. *Reviews of Accelerator Science and Technology*, *4*, 11-40.

Mahne, N., Čekada, M., & Panjan, M. (2022). Total and differential sputtering yields explored by SRIM simulations. *Coatings*, *12*(10), 1541.

Mahne, N., Čekada, M., & Panjan, M. (2023). Energy distribution of sputtered atoms explored by SRIM simulations. *Coatings*, *13*(8), 1448.

Nastasi, M., Mayer, J.W., & Hirvonen, J.K. (1996). *Ion-solid interactions: fundamentals and applications*. Cambridge University Press, New York.

Nath, D., & Das, R. (2021). Surface and displacement damage engineering on CdSe nanocrystalline thin film by swift heavy Ag ions: a theoretical investigation by SRIM/TRIM package. *Vacuum*, *190*, 110293.

Nordlund, K., Sand, A.E., Granberg, F., Zinkle, S.J., Stoller, R., Averback, R.S., Averback, R.S., Suzudo, T., Malerba, L., Banhart, F., Weber, W.J., Willaime, F., Dudarev, S., & Simeone, D. (2015). Primary radiation damage in materials. Review of current understanding and proposed new standard displacement damage model to incorporate in cascade defect production efficiency and mixing effects. *Nuclear Energy Agency*, *9*, 1-11.

Nordlund, K., Zinkle, S.J., Sand, A.E., Granberg, F., Averback, R.S., Stoller, R., Suzudo,T., Malerba, L., Banhart, F., Weber, W.J., Willaime, F., Dudarev, S.L., & Simeone, D. (2018). Improving atomic displacement and replacement calculations with physically realistic damage models. *Nature Communications*, *9*(1), 1084.

Racz, A.S., Kun, P., Kerner, Z., Fogarassy, Z., & Menyhard, M. (2023). Tungsten carbide nanolayer formation by ion beam mixing with argon and xenon ions for applications as protective coatings. *ACS Applied Nano Materials*, *6*(5), 3816-3824.

Ramola, R.C., Semwal, A., Negi, A., Joshi, V., & Singh, F. (2013). Effects of Li3+ and Ni9+ Ion beams on polyether sulfone polymer. *Advances in Polymer Technology*, *32*(3), 21361-21368. https://doi.org/10.1002/adv.21360.

Rautray, T.R., Narayanan, R., & Kim, K.H. (2011). Ion implantation of titanium based biomaterials. *Progress in Materials Science*, *56*(8), 1137-1177.

Robinson, M.T. (1994). Basic physics of radiation damage production. *Journal of Nuclear Materials*, *216*, 1-28.

Seitz, F. (1956). Displacement of atoms during irradiation. *Solid State Physics*, *2*, 305-449.

Seyyedhabashy, M.M., Tafreshi, M.A., Shafiei, S., & Nasiri, A. (2020). Damage studies on irradiated tungsten by helium ions in a plasma focus device. *Nuclear Engineering and Technology*, *52*(4), 827-834.

Shu, X., Tao, P., Li, X., & Yu, Y. (2013). Helium diffusion in tungsten: a molecular dynamics study. *Nuclear Instruments and Methods in Physics Research Section B: Beam Interactions with Materials and Atoms*, *303*, 84-86.

Sigmund, P. (1981). Sputtering by ion bombardment theoretical concepts. In: Behrisch, R. (ed) *Sputtering by Particle Bombardment I*. Topics in Applied Physics (vol 47). Springer, Berlin, Heidelberg. https://doi.org/10.1007/3540105212_7.

Sigmund, P. (2014). Particle penetration and radiation effects (vol. 2). In *Springer series in solid-state sciences* (Vol. 179). Springer, Heidelberg.

Singh, S., & Rout, B. (2021). Simulation study of surface sputtering and distribution of ions in silicon due to low-energy high-fluence cobalt irradiation. *Surfaces and Interfaces*, *24*, 101035.

Stoller, R.E. (2012). Primary radiation damage formation. *Comprehensive Nuclear Materials*, *1*, 293-332.

Stoller, R.E., Toloczko, M.B., Was, G.S., Certain, A.G., Dwaraknath, S., & Garner, F.A. (2013). On the use of SRIM for computing radiation damage exposure. *Nuclear Instruments and Methods in Physics Research Section B: Beam Interactions with Materials and Atoms*, *310*, 75-80.

Weber, W.J., & Zhang, Y. (2019). Predicting damage production in monoatomic and multi-elemental targets using stopping and range of ions in matter code: challenges and recommendations. *Current Opinion in Solid State and Materials Science*, *23*(4), 100757.

Zhu, F., Chen, Z.L., Liu, K.Z., Liang, W., & Zhang, Z. (2018). Deposition of thin tungsten carbide films by dual ion beam sputtering deposition. *Vacuum*, *157*, 45-50.

Ziegler, J.F., & Biersack, J.P. (1985). The stopping and range of ions in matter. In Allan, B.D. (ed) *Treatise on Heavy-Ion Science: Astrophysics, Chemistry, and Condensed Matter* (Vol. 6, pp. 93-129). Springer, Boston, MA, US.

Ziegler, J.F., Ziegler, M.D., & Biersack, J.P. (2010). SRIM–The stopping and range of ions in matter (2010). *Nuclear Instruments and Methods in Physics Research Section B: Beam Interactions with Materials and Atoms*, *268*(11-12), 1818-1823.

Ziegler, J.F., & Biersack, J.P. (2008). SRIM-2008, stopping power and range of ions in matter. http://inis.iaea.org/Search/search.aspx?orig_q=RN:40107606'.



**Publisher's Note**- Ram Arti Publishers remains neutral regarding jurisdictional claims in published maps and institutional affiliations.